Progress In Electromagnetics Research, PIER 34, 313–333, 2001

APPLICABILITY OF COMBINED MICROWAVE AND OPTICAL DATA FOR SURFACE WATER QUALITY RETRIEVALS

Y. Zhang, J. Pulliainen, S. Koponen, and M. Hallikainen

Helsinki University of Technology
Laboratory of Space Technology
P.O. Box 3000, 02015 HUT, Finland

Abstract—This paper presents the applicability of combined microwave (ERS-2 SAR) and optical (Landsat TM) data for surface water quality retrievals. Three surface water quality parameters such as turbidity, Secchi disk depth (SDD), and suspended sediment concentration (SSC) in the Gulf of Finland are estimated using multivariate approach. The results indicate that the visible bands of TM data are somewhat correlated to SAR signals, by which SAR can explain 14.4% of the variability in TM2 observations. Multivariate analyses show that SAR has some contribution to derive those parameters if they are somewhat correlated to the water surface properties. Although it may be possible to develop algorithms for surface water quality retrievals in which SAR is used as supplementary data to optical observations, it still needs to be refined sufficiently to detect differences within the range of these parameters in the area under study.

1. INTRODUCTION

It is well known that sea surface properties can be imaged by microwave signals such as synthetic aperture radar (SAR) carried by aircrafts or satellites [1–8]. Presently, a wavelength 5.3 cm SAR (C-band) is flown on the European Remote Sensing Satellite (ERS-1/2), which is designed to image ocean surface waves globally [9]. One major advantage of microwaves over other windows in the electromagnetic spectrum is that microwaves are not hindered by clouds. At microwave frequencies, the sea surface is almost a perfect conductor. As a result, the microwave radiation penetrates only one-tenth of a wavelength into the water column, which is about 5 mm for the ERS-1/2 SAR. Since all features visible in SAR imagery of the sea are necessarily surface phenomena, all structures in ERS-2 SAR images are related to changes in the surface roughness [10].

On the other hand, optical data at visible and near infrared (IR) wavelengths such as Landsat information have been used to evaluate surface water quality since 1970's [11, 12]. Observations of such surface water quality parameters as turbidity, Secchi disk depth, and suspended sediment concentration provide quantitative information concerning surface water quality conditions and are also used in various numerical schemes to help characterise the trophic state of an aquatic ecosystem [13]. However, the number of available *in situ* measurements of surface water quality characteristics is usually limited, especially in temporal and spatial domains, due to the high costs of data collection and laboratory analysis [14]. The literature suggests that Landsat TM data can provide an alternative method to obtain relatively low-cost, simultaneous information on surface water conditions for numerous lakes and large coastal or oceanic areas [15–19].

The coastal waters in the Gulf of Finland are dominated by absorption from both dissolved and particulate organic matter, whereas the Gulf is optically dominated by scattering from suspended sediments. This is because the whole Gulf is highly affected by the input from the rivers that have a high concentration of mineral suspended solids and nutrients. Such optical characteristics of the water have been studied by using optical remote sensing data in the area [20, 21].

In this study, we investigate the applicability of combined microwave (ERS-2 SAR) and optical (Landsat TM) data over the Gulf of Finland. Three surface water quality parameters such as turbidity, Secchi disk depth and suspended sediment concentration are also retrieved using a multivariate approach in the study area.

2. REMOTE SENSING THEORY

In remote sensing, physical phenomena are observed through properties and changes in electromagnetic (EM) radiation. This means that EM waves are carriers of information, and an understanding of their interaction with matter is necessary. EM waves have the following measurable properties: frequency or wavelength, polarisation, and phase. The different interactions of waves with a surface or volume can be listed as: emission, absorption, reflection (scattering), refraction, and transmission.

A fundamental fact is that all natural bodies emit incoherent radiant EM energy. Moreover, the energy radiated by the Sun is reflected, absorbed and scattered from atmosphere as well as all natural bodies. A simplified theoretical schema involving this radiation mechanism can be set up. This basic measurement configuration is shown in Figure 1. The field of view (FOV) of the observer is shown as dashed lines. The signal received by the observer has components from the surface (L_{surf}), the atmosphere (L_{atm}), a reflected component (L_{refl}) and a secondary refracted component (L_{refr}). Depending on the measured wavelength, some components are dominant. In the case of active sensing, the geometry changes so that L comes from the direction of the observer, and the received signal is mainly constituted of a reflected wave (L_{refl}), possibly a refracted wave (L_{refr}), while L_{surf} and L_{atm} are insignificant. The emitted energy, marked L_{surf}, comes from the surface of the body itself. Therefore, the signal (L_{up}) received by the observer can be approximately expressed as:

$$L_{up} = L_{refl} + L_{refr} \tag{1}$$

Planck's blackbody radiation law defines the radiated spectral brightness $B_f(W/m^2sr^1Hz)$ as:

$$B_f = \frac{2hf^3}{c^2}\left(\frac{1}{e^{\frac{hf}{kT}} - 1}\right) \tag{2}$$

where k is Planck's constant, T is the physical temperature of the body and f is frequency. Usually, a derived measure, the brightness

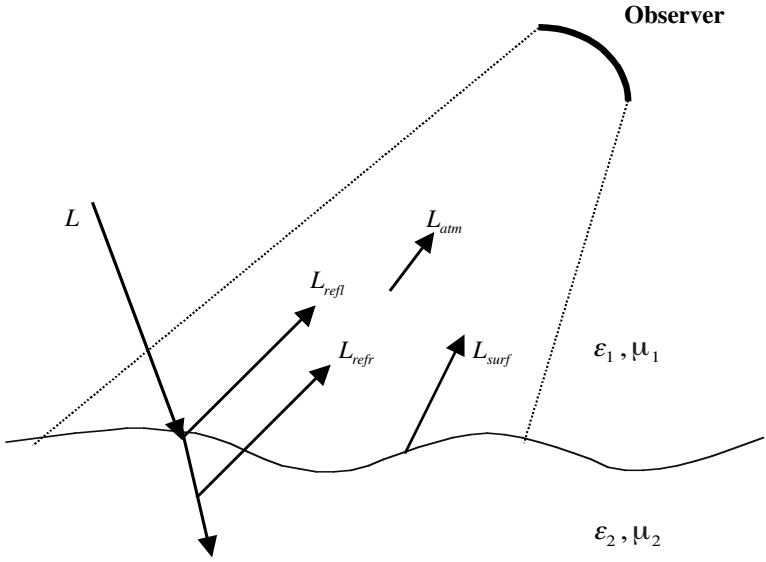

Figure 1. A basic remote sensing setup configuration.

temperature T_b is used instead. The brightness temperature T_b represents the intensity of the observed radiation and is defined as:

$$T_b(\varphi, \theta) = eT(\varphi, \theta) \tag{3}$$

where e is the emissivity of the medium and T is physical temperature. The emissivity is a value between 0 and 1 and, theoretically, can be 0 for a perfect conductor and 1 for a perfect black body. For all natural objects it is less than 1, therefore the brightness temperature is always lower than the physical temperature. Furthermore, the emissivity is a function of frequency and material properties, of which the dielectric coefficient of the medium is the most significant when using microwaves. Also, it should be noted that the brightness temperature is dependent on the angle of observation as shown in Figures 2(a) and 2(b).

The component marked as L_{refl} in Figure 1 represents reflected energy from an outside source. Part of this energy will be absorbed and eventually refracted, marked L_{refr}. The reflection phenomena can be approximated using two parts: specular reflection and scattering from a rough surface. These two components are represented in Figure 3(a) and 3(b). In the specular case of Figure 3(a), the reflection coefficient r_0 can be determined using the elementary Fresnels' formulas. Briefly,

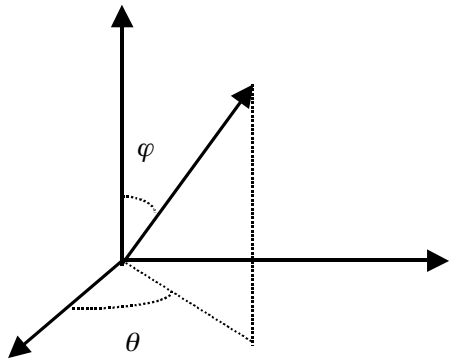

Figure 2a. Coordinate system for Figure 2(b).

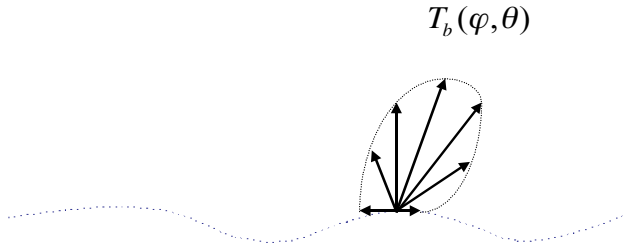

Figure 2b. The brightness temperature distribution of a semi-infinite isothermal medium.

these formulas can be expressed as dependencies in the following way:

$$r_0 = r_0(p, \varepsilon_r, \theta) \tag{4}$$

That is, they are functions of polarisation p, dielectric permittivity ε_r, and incident angle θ.

However, scattering from a rough surface is more complex and highly dependent on observed wavelength. Theoretical, semi-empirical and empirical models can be found in literature [22–25]. A simple semi-empirical model will be presented here to grasp an overview of the problem. The scattered component S (including coherent and incoherent contributions) can be expressed as:

$$S = r_0 P_i G \tag{5}$$

In Figure 3(b) is carrying the incoming wave P_i, the specular reflection factor r_0 and unknown function G. The latter can be expanded in an exponential function with F dependent on wavelength, incoming angle,

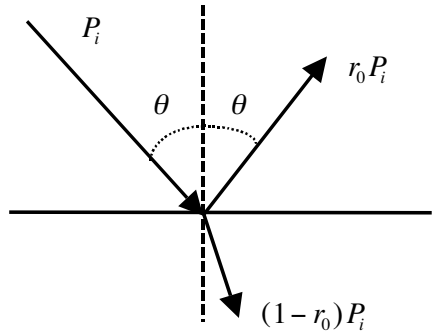

Figure 3a. Specular reflection and transmission.

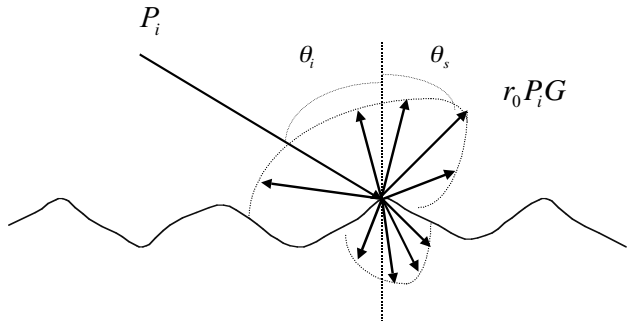

Figure 3b. Scattering and transmission from a rough surface.

rms. height of surface roughness, and polarisation. That is, G could resemble at something like

$$G = \exp[F(\lambda, \sigma_h, \theta, p)] \tag{6}$$

where λ is the wavelength, σ_h is the rms. deviation of roughness, θ is the incident angle and p is a polarisation coefficient. Because the roughness is determined by the wavelength used to make measurements, a more precise approach would be needed for different remote sensing instruments. So far, the components marked L_{atm} in Figure 1 has been ignored. It represents the emissivity and scattering of the atmosphere, which will be skipped here.

3. APPLICABILITY OF COMBINED SAR AND TM

One comparison of nearly simultaneous one scene space-borne optical and microwave water area observations was possible for one occasion,

16 August 1997. On that date, the Landsat TM sensor and the ERS-2 SAR imaged the same coastal region at 8.44 UTC and 9.40 UTC, respectively. Since the time difference between the imaging was less than one hour, the water surface wave conditions, including wind and water temperature, can be assumed to be quite similar for both images (spatial differences in wave conditions). In the past 24 hours, the average wind speed is about 5.5 m/s with the Northwest wind direction. The average surface water temperature is about 19.5 C degrees and the average wave height is about 0.39 m.

The key characteristics affecting microwave radar observations, in addition to water dielectric constant, are the water surface roughness properties. Since water mass below the surface does not contribute to the microwave radar backscattering, actual water quality characteristics do not directly influence these radar observations. Therefore, the signal (L_{up}) received by Radar can be approximately expressed as:

$$L_{up} = L_{refl} \tag{7}$$

At optical wavelengths, however, radiation detected by a remote sensing instrument includes both the contribution scattered inside the water body and the contribution reflected from the water surface. Therefore, bi-directional reflection of Sun radiation from the water surface is in the case of optical data merely a factor disturbing the actual water quality retrieval [26].

These optical remote observations are affected by the atmosphere and radiation from the direct reflectance due to the water surface. These effects must be removed with suitable atmospheric correction and bidirectional reflectance models before data analysis. When Landsat TM data are used to retrieve quantitative data concerning the water surface, it is necessary to correct atmospheric effects [27, 28].

The radiance energy observed by a sensor with the hypothesis of homogeneous ground reflectance consists of several components, and can be expressed:

$$L_{sat} = T_r(L_{atm} + L_{up}) \tag{8}$$

and

$$L_{up} = L_{refr} + L_{refl} = L_w + L_{refl} \tag{9}$$

where L_{sat} is the radiance gathered by the sensor, and T_r is the atmospheric transmittance due to absorption by atmospheric gases such as ozone, water vapor, carbon dioxide and molecular oxygen. L_{atm} is the atmospheric radiance due to light scattering from gases and aerosols and L_{up} is the radiance directly coming from the ground target. L_w is the radiance refracted from inside the water body while

L_{refl} is the radiance reflected from the water surface. Here, in the case of water, L_{refr} is substituted by L_w. So far, the radiance emitted from the surface of water body itself (L_{surf}) has been ignored.

However, if no atmospheric measurements are available, the appropriate correction value for each spectral band can be determined in a simple algorithm by histogram inspection and thus setting the minimum value to zero, i.e., a simple shifting of values. This approach is valid knowing that atmospheric scattering is the dominating effect compared to absorption caused by the atmosphere in the shorter wavelengths, e.g., TM bands 1–3. Another technique is to observe a reflectance target such as deep, clear water, a "dark object" [29], later improved by the same author Chavez [30], that should almost completely absorb all light in the near IR wavelength region, and thus should have brightness values close to zero [31]. Since the atmospheric correction has no effects on correlation analysis in a single TM image, the atmospheric correction could be ignored if it is in the case of only one scene TM.

In order to eliminate the effect of incidence/reflection angle variation inside the TM and SAR image, the spatial range in investigations was limited to 60 km (across track range for both images). Moreover, an angular correction was made for SAR signatures (normalization to the incidence angle of 19.5°). This was done due to the strong dependence of water surface backscattering on the angle of incidence, which is evident for ERS-2 SAR data even for as small spatial range as 60 km. The correction was performed by applying an exponential model given by Ulaby et al. [32].

4. RETRIEVAL METHOD

4.1. Multivariate Approach

At the optical wavelengths, passive remote sensing observations are affected by the volume scattering inside the water body and the reflection from the water surface. However, radar measurements are only affected by water surface properties. The temporal and spatial variations in water surface roughness are actually factors that disturb the interpretation of optical data [33]. Since the radar observations are only influenced by the surface layer, it may be possible to develop an algorithm to estimate water quality parameters in which SAR data are used as supplementary data to optical observations.

In this study, multivariate retrieval algorithms for surface water quality parameters using either TM data or combined SAR/TM data

can be expressed as follows:

$$D_{TM} = A_0 + \sum_{i=1}^{k} A_i(TM_i) \quad (10)$$

$$D_{TM/SAR} = A_0 + \sum_{i=1}^{k} (TM_i) + A(SAR) \quad (11)$$

where TM_i and SAR are the digital number (DN) values of 7 TM bands and single ERS-2 channel, k is the TM band number from 1 to 7, and A_0, A_i, and A are the empirical regression coefficients derived by using the observations from the ground truth points.

4.2. Validation against In Situ Data

The capability of satellite remote sensing to yield synoptic information of water quality over large areas is a valuable tool. Also, it is important that the information of water quality obtained from satellite remote sensing is supported by *in situ* measurements. However, the limitation of this technology is that the accuracy of water quality information derived from that is based on *in situ* sampling only [34, 35]. Therefore, the validation of turbidity against *in situ* data ranges from 1.0 to 7.5 FTU, while the validation of SDD against *in situ* data is from 0.67 to 4.2 meters and that of suspended sediment concentration against *in situ* data ranges from 1.6 to 11.0 mg/l in this study.

5. RESULTS AND DISCUSSION

A previous examination of the correlation (r^2) between turbidity and chlorophyll-a is 0.06. This suggested that the turbidity in the Gulf of Finland was not dependent on plankton biomass [36]. However, the correlation of turbidity with suspended sediment concentration (SSC) is up to 0.81, which implies that turbidity is significantly related to suspended sediments in the Gulf. On the other hand, SDD has a correlation (r^2) of 0.31 with chlorophyll-a and that of 0.49 with SSC. This means that SDD is weakly but somewhat correlated to both dissolved and particulate organic matter in the study. Examination of the correlations (r^2) between observed intensities at different TM bands ranged from 0.001 to 0.933 [37]. This difference among TM bands implies that these bands may either change highly at any site or change differently at all sites. Furthermore, the high relationship between bands are measuring similar surface water properties in the study.

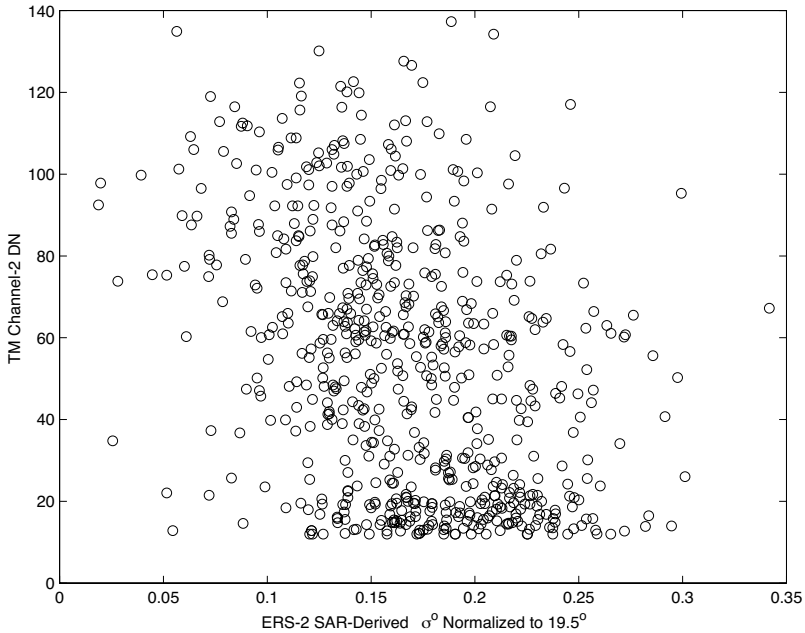

Figure 4. Behavior of observed TM2 intensity as a function of observed C-band ERS-2 SAR backscattering coefficient ($r = -0.38$) (661 points).

The results indicate that the data from visible bands of TM are to a degree correlated with the C-band ERS-2 SAR observations [37]. The highest correlation (r^2) of 0.144 is between SAR data and TM2. Since angular corrected SAR observations are only dependent on the surface wave conditions (in addition to random speckle, which was mostly averaged out in the employed water area signatures), this may suggest that SAR can explain 14.4% of the variability in TM2 observations (Fig. 4), by which TM2 is low but somewhat correlated to the water surface properties.

Simple regression analyses for turbidity, Secchi disk depth (SDD) and suspended sediment concentration (SSC), in relation to TM bands and SAR data, were also analysed [37]. All visible and near-IR bands (Bands 1–4) were low but somehow predictive of turbidity with the exception of the TM5, TM6 and TM7. Variations in the turbidity were most adequately explained by TM3, which explained 66% of the variation in a low but significant regression. These same bands also show similar predictive of the variations in both SDD and SSC, although no single variable explained more than 53% of these two

variations. On the other hand, SAR explained 36.8% of the SDD, while SAR only explained 5% of the turbidity and 9% of the SSC.

The results of using TM band ratios, band differences, logarithmic transformations, chromaticity analyses and some other combinations of visible and near-IR bands (TM 1–4) were also compared [37]. All these numerous transformations did not improve the retrieval accuracy than simple regression analyses.

5.1. Turbidity Retrieval

Turbidity is one important optical measurement of surface water quality. Since there is no real standard as how to record turbidity, most measurements of turbidity are incomparable. This means that they cannot be translated into other units of turbidity measurements. However, almost all measures of turbidity can give a high correlation to satellite optical signatures.

According to equations (10) and (11), multivariate approach for turbidity (*Turb*) can be expressed as in this study:

$$\begin{aligned} Turb = {} & 4.1106 - 0.0346(TM1) + 0.0294(TM2) + 0.1123(TM3) \\ & +0.5137(TM4) - 0.2775(TM5) - 0.0204(TM6) - 0.0324(TM7) \end{aligned} \tag{12}$$

with the coefficient of determination ($R^2 = 0.709$) and with the root mean square error (RMSE = 0.794 FTU).

As ERS-2 SAR data is used in addition to TM data we obtain:

$$\begin{aligned} Turb = {} & 4.1024 - 0.0346(TM1) + 0.0294(TM2) + 0.1120(TM3) \\ & +0.5143(TM4) - 0.2781(TM5) - 0.0204(TM6) \\ & -0.0323(TM7) + 0.0000(SAR) \end{aligned} \tag{13}$$

with the coefficient of determination ($R^2 = 0.709$) and with (RMSE = 0.794 FTU) (Fig. 5). Both of these regressions explained 70.9% of the variation with a root mean square error (RMSE) of 0.794 FTU. The results show that turbidity algorithm derived using combined TM 7 bands with SAR is same as that using TM data. This means that the SAR does not improve the turbidity retrieval accuracy.

The summary of multivariate turbidity algorithms from combined TM bands and SAR data, as well as the comparison with those from TM data, is presented in Table 1. The results demonstrate that the accuracy of turbidity estimation using combined TM/SAR data is not higher than that using TM data. This is because the SAR is very little correlated to the turbidity ($r^2 = 0.055$). This probably means that the turbidity is not related to the water surface properties in

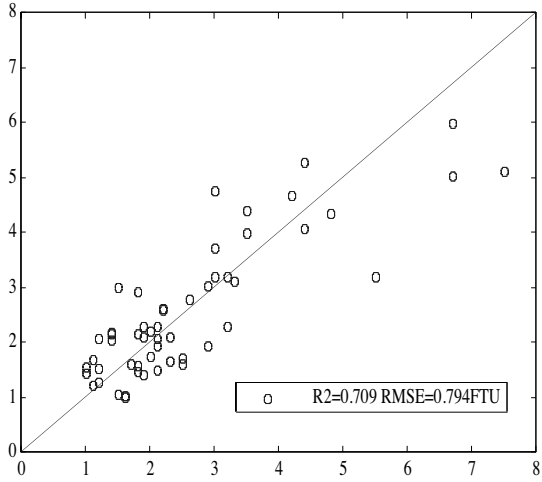

Figure 5. Regression of turbidity measured estimated from combined SAR/TM.

the study material. Although the turbidity retrieval accuracy using a multivariate approach (70.9%) is slightly better than a single band regression (66%), this small improvement is not very helpful to retrieve turbidity for the practical use in our study area.

5.2. Secchi Disk Depth Retrieval

Secchi disk depth (SDD) is another important optical measurement concerning surface water quality. So far, SDD has become a universally accepted tool to measure water transparency.

Using equations (10) and (11), the SDD can be written as:

$$SDD = 1.8780 + 0.0427(TM1) + 0.0017(TM2) - 0.1419(TM3) - 0.2562(TM4) + 0.0185(TM5) + 0.0085(TM6) + 0.0054(TM7) \quad (14)$$

with the coefficient of determination ($R^2 = 0.740$) and (RMSE = 0.441 m) or as ERS-2 SAR data is also applied:

$$SDD = 3.4515 + 0.0294(TM1) - 0.0097(TM2) - 0.0791(TM3) - 0.3750(TM4) + 0.1268(TM5) + 0.0074(TM6) - 0.0104(TM7) - 0.0031(SAR) \quad (15)$$

Table 1. The summary of turbidity (*Turb*) derived from TM bands and from combined TM/ERS-2 SAR data (53 points).

	TURBIDITY (Turb)										
ALGORITHM	TM1	TM2	TM3	TM4	TM5	TM6	TM7	ERS	CON	R^2	RMSE
Eq. (10), k=7	-0.0346	0.0294	0.1123	0.5137	-0.2775	-0.0204	-0.0324	-	4.1106	0.709	0.794
Eq. (11), k=7	-0.0346	0.0294	0.1120	0.5143	-0.2781	-0.0204	-0.0323	0.0000	4.1024	0.709	0.794
Eq. (10), k=4	-0.0305	0.0367	0.0952	0.0636	-	-	-	-	0.6909	0.681	0.830
Eq. (11), k=4	-0.0325	0.0345	0.1054	0.0612	-	-	-	-0.0005	0.9338	0.682	0.829
Eq. (10), k=3	-0.0307	0.0355	0.1015	-	-	-	-	-	0.8245	0.681	0.830
Eq. (11), k=3	-0.0328	0.0333	0.1119	-	-	-	-	-0.0005	1.0699	0.682	0.830

Note: CON = Constant, R^2 = Regression, RMSE = Root mean square error

with the coefficient of determination ($R^2 = 0.774$) and (RMSE = 0.412 m) (Fig. 6). The latter regression explained 77.4% of the variation in SDD with RMSE of 0.412 m. The results show that the accuracy of SDD using combined TM/SAR is slightly higher than that of using TM (74% of the variation with an RMSE of 0.441 m). This probably implies that SDD is somewhat correlated to the surface water properties in this study.

The summary of SDD derived from combined TM bands and SAR data, as well as the comparison with those from TM bands, is presented in Table 2. The results show that the SDD accuracy estimated from combined TM/SAR data is slightly better than that from TM bands. This is because SAR has a low but significant correlation ($r^2 = 0.368$) with the SDD. The results also suggest that there are some microwave backscattering signatures corresponding to SDD in this study. Moreover, the SDD retrieval accuracy using multivariate approach (77.4%) is much better than a single band regression of SDD (53%). This high improvement (24.4%) probably implies that the multivariate approach is very helpful to retrieve the SDD for practical use in the study area.

Table 2. The summary of Secchi disk depth (SDD) derived from TM bands and from combined TM/ERS-2 SAR data (53 points).

	SECCHI DISK DEPTH (SDD)										
ALGORITHM	TM1	TM2	TM3	TM4	TM5	TM6	TM7	ERS	CON	R^2	RMSE
Eq. (10), k=7	0.0427	0.0017	-0.1419	-0.2562	0.0185	0.0085	0.0054	-	1.8780	0.740	0.441
Eq. (11), k=7	0.0294	-0.0097	-0.0791	-0.3750	0.1268	0.0074	-0.0104	-0.0031	3.4515	0.774	0.412
Eq. (10), k=4	0.0404	0.0017	-0.1374	-0.1898	-	-	-	-	3.0962	0.731	0.449
Eq. (11), k=4	0.0283	-0.0112	-0.0768	-0.2039	-	-	-	-0.0030	4.5298	0.763	0.421
Eq. (10), k=3	0.0410	0.0052	-0.1563	-	-	-	-	-	2.6979	0.724	0.454
Eq. (11), k=3	0.0291	-0.0073	-0.0982	-	-	-	-	-0.0029	4.0762	0.755	0.429

Note: CON = Constant, R^2 = Regression, RMSE = Root mean square error

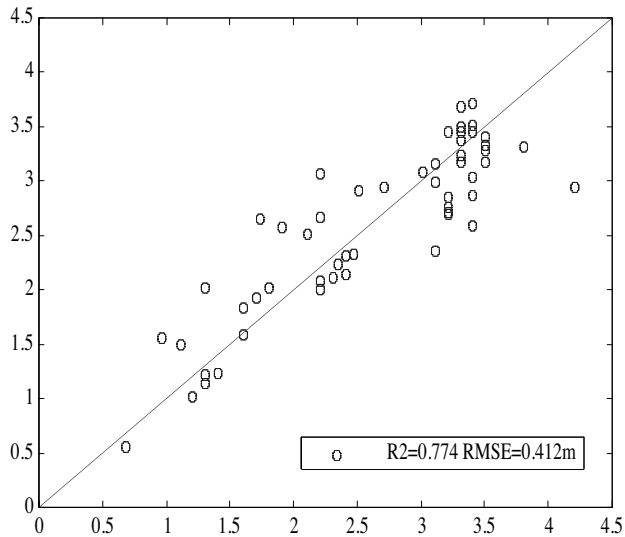

Figure 6. Regression of SDD measured with estimated from combined SAR/TM.

5.3. Suspended Sediment Concentration Retrieval

Suspended sediment concentration is one of most successfully measured parameters by means of remote sensing. Theoretically, a suspension of inorganic matter of a homogeneous fraction should give the most accurate model results of all substances in a water mass as this material has well defined physical reflectance properties [33].

Even a small concentration of suspended sediment increases the volume reflectance in a manner that becomes more pronounced as the wavelength becomes longer. Reflectance increases with suspended sediment concentration and peak reflectance shifts to higher wavelengths with increasing concentrations. At high concentrations of suspended sediments, where the relationship between reflectance and suspended sediment departs from being linear, the radiance resolution decreases noticeably. Thus, the accuracy of suspended sediment concentration estimation decreases [33]. At very large concentrations of suspended sediment, the volume reflectance spectrum displays an asymptotic approach to a broad peak around 700 nm (red region) [38].

Using equation (10) and (11), suspended sediment concentration (SSC) can be estimated by:

$$\begin{aligned} SSC = {} & 8.6880 - 0.0221(TM1) - 0.0202(TM2) + 0.2831(TM3) \\ & -0.2822(TM4) + 0.3639(TM5) - 0.0405(TM6) - 0.2579(TM7) \end{aligned} \tag{16}$$

with the coefficient of determination ($R^2 = 0.572$) and with the root mean square error (RMSE = 1.416 mg/l) or as ERS-2 SAR is also employed:

$$\begin{aligned} SSC = {} & 7.0587 - 0.0084(TM1) - 0.085(TM2) + 0.2181(TM3) \\ & -0.1592(TM4) - 0.2518(TM5) - 0.0394(TM6) \\ & -0.2416(TM7) + 0.0033(SAR) \end{aligned} \tag{17}$$

with the coefficient of determination ($R^2 = 0.578$) and (RMSE = 1.406 mg/l) (Fig. 7). The latter regression explained 57.8% the variation in SSC with an RMSE of 1.406 mg/l. These results show that SSC derived using TM 7 bands with SAR data is very little improved the SSC retrieval accuracy.

The summary of SSC estimated from combined TM/SAR data, as well as the comparison with those from TM data, is presented in Table 3. The results show that the accuracy of SSC derived from combined TM/SAR data is very little better (0.6%) than that from TM bands in our study. This is because SAR has a very low correlation ($r^2 = 0.098$) with SSC. The results probably suggest that SSC is also

Table 3. The summary of suspended sediment concentration (SSC) derived from TM bands and from combined TM/ERS-2 SAR data (53 points).

	SUSPENDED SEDIMENT CONCENTRATION (SSC)										
ALGORITHM	TM1	TM2	TM3	TM4	TM5	TM6	TM7	ERS	CON	R^2	RMSE
Eq. (10), k=7	-0.0221	-0.0202	0.2831	-0.2822	0.3639	-0.0405	-0.02579	-	8.6880	0.572	1.416
Eq. (11), k=7	-0.0084	-0.0085	0.2181	-0.1592	0.2518	-0.0394	-0.2416	0.0033	7.0587	0.578	1.406
Eq. (10), k=4	-0.0146	-0.0225	0.2662	-0.3199	-	-	-	-	2.4308	0.545	1.460
Eq. (11), k=4	-0.0004	-0.0074	0.1953	-0.3034	-	-	-	0.0035	0.7543	0.552	1.449
Eq. (10), k=3	-0.0135	-0.0166	0.2243	-	-	-	-	-	1.7594	0.542	1.465
Eq. (11), k=3	0.0009	-0.0015	0.1635	-	-	-	-	0.0035	0.0795	0.549	1.454

Note: CON = Constant, R^2 = Regression, RMSE = Root mean square error

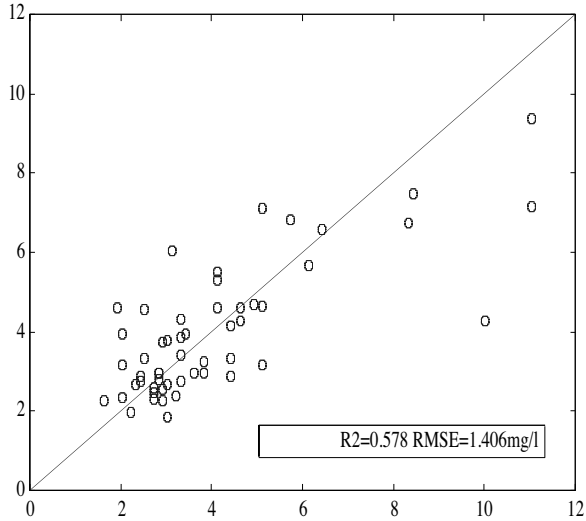

Figure 7. Regression of SSC measured with estimated from combined SAR/TM.

not significantly correlated to the water surface properties in the study. Although the SSC retrieval accuracy using a multivariate approach (57.8%) is slightly better than a single band regression of SSC (53%), this small improvement (4.8%) is not very helpful to retrieve the SSC for the practical use in our case study.

The results of SSC estimation are not so good as in some other studies, for example Tassan [39] derived logarithm of total suspended sediment from ln(TM2) with the determination of $r^2 = 0.92$. A probable reason is that the coastal waters in the study area, where the surface water properties are actually in non-linear behavior, are optically dominated by absorption from both dissolved and particulate organic matter. Such a reason will be further studied in the future.

6. CONCLUSION

In this study, we investigated the applicability of combined microwave (ERS-2 SAR) and optical (Landsat TM) data for surface water quality retrievals over the Gulf of Finland. The in situ surface water quality measurements and the corresponding data sets of SAR and TM were used to derive three surface water parameters such as turbidity, Secchi disk depth and suspended sediment concentration. The TM and SAR data from locations of water samples were extracted and digital data were examined in their raw states as well as numerous transformations. Low but significant correlations were observed between the digital data and the three surface water parameters. The results indicate that the visible bands of TM are to a degree correlated to SAR, by which SAR can explain 14.4% of the variability in TM2 observations. The results of multivariate analyses show that SAR has no supplementary value to retrieve those parameters if such parameters are not correlated to water surface properties. The results suggest that SAR is no (or very little) contribution to turbidity and SSC retrievals. That is, both of turbidity and SSC are not (or very little) correlated to the water surface properties in this study. On the other hand, the retrieval accuracy of SDD derived from combined TM/SAR data is slightly better than that from TM. This probably means that SAR has a few contributions to SDD retrievals, since SDD is somewhat correlated to the water surface properties. A probable reason is that the surface water properties in the study area are in non-linear behavior in that the coastal waters over the Gulf of Finland are optically dominated by absorption from both dissolved and particulate organic matter. Therefore, the technique still needs to be refined sufficiently to detect differences within the range of surface water quality parameters in the area.

ACKNOWLEDGMENT

The authors would like to thank K. Eloheimo, K. Kallio, T. Hannonen, P. Härmä, T. Kutser, T. Pyhälahti, J. Vepsäläinen, Y. Sucksdorff, J. Kämäri, J. Vuorimies, H. Servomaa and S. Tauriainen for providing necessary supports.

REFERENCES

1. Alpers, W., D. B. Ross, and C. L. Rufenach, "On the detectability of ocean surface waves by real and synthetic aperture radar," *J. Geophys. Res.,* Vol. 86, 6481–6498, 1981.
2. Shuchman, R. A. and O. H. Shemdin, "SAR imaging of the ocean surface waves during the Marineland experiment," *IEEE J. Oceanic Eng.,* Vol. OE-8, 83–90, 1981.
3. Vesecky, J. F. and R. H. Stewart, "The observation of ocean surface phenomena using imagery from SAESAT synthetic aperture radar: an assessment," *J. Geophys. Res.,* Vol. 87, 3397–3430, 1982.
4. Beal, R. C., D. G. Tilley, and F. M. Monaldo, "Large and small scale spatial evolution of digitally processed ocean wave height spectra from SEASAT synthetic aperture radar," *J. Geophys. Res.,* Vol. 88, 1761–1778, 1983.
5. Hasselmaan, K., R. K. Raney, W. J. Plant, W. Alpers, R. A. Shuchman, D. R. Lyzenga, C. L. Rufenach, and M. J. Tucker, "Theory of SAR ocean wave imaging, a MARSEN view," *J. Geophys. Res.,* Vol. 90, 4659–4686, 1985.
6. Monaldo, F. M. and D. R. Lyzenga, "On the estimation of wave slope- and height-variance spectra from SAR imagery," *IEEE Trans. Geosci. Remote Sens.,* Vol. GE-24, 543–551, 1986.
7. Bruning, C., W. Alpers, L. F. Zambresky, and D. G. Tilley, "Validation of a synthetic aperture radar ocean wave imaging theory by the Shuttle Imaging Radar-B experiment over the North Sea," *J. Geophys. Res.,* Vol. 93, 15,403–15,425, 1988.
8. Nilsson, C. S. and P. C. Tildesley, "Imaging of oceanic features by ERS-1 synthetic aperture radar," *J. Geophys. Res.,* Vol. 100, 953–967, 1995.
9. Bruning, C., R. Schmidt, and W. Alpers, "Estimation of the ocean wave-radar modulation transfer function from synthetic aperture radar imagery," *J. Geophys. Res.,* Vol. 99, 9803–9815, 1994.
10. Vogelzang, J., "Mapping submarine sand waves with multiband

imaging radar, 1. Model development and sensitivity and analysis," *J. Geophys. Res.,* Vol. 102, 1163–1181, 1997.

11. Klemas V., D. Bartlett, W. Philpot, and R. Roger, "Coastal and estuarine studies with ERTS-1 and Skylab," *Remote Sens. Environ.,* Vol. 3, 153–177, 1974.
12. Alföldi, T. and J. C. Munday, "Water quality analysis by digital chromaticity mapping of Landsat data," *Canadian J. Remote Sens.,* Vol. 4, 108–122, 1978.
13. Carlson, R. E., "A trophic state index for lakes," *Limnol. Oceanogr.,* Vol. 22, 361–369, 1977.
14. Harrrington Jr., J. A. and F. R. Schiebe, "Remote sensing of Lake Chicot, Arkansas: monitoring suspended sediments, turbidity, and secchi depth with Landsat MSS data," *Remote Sens. Environ.,* Vol. 39, 15–27, 1992.
15. Lathrop Jr., R. G. and T. M. Lillesand, "Use of Thematic Mapper data to assess water quality in Green Bay and central Lake Michigan," *Photogramm. Eng. Remote Sens.,* Vol. 52, 671–680, 1986.
16. Doerffer, R., J. Fischer, M. Stossel, and C. Brockmann, "Analysis of Thematic Mapper data for studying the suspended matter distribution in the coastal area of the Germany Bight (North Sea)," *Remote Sens. Environ.,* Vol. 28, 61–73, 1989.
17. Lathrop, R. G., T. M. Lillesand, and B. S. Yandell, "Testing the utility simple multi-date Thematic Mapper calibration algorithms for monitoring turbid inland waters," *Int. J. Remote Sens.,* Vol. 12, 2045–2063, 1991.
18. Dekker, A. G. and S. W. M. Peters, "The use of the Thematic Mapper for the analysis of eutrophic lakes: a case study in the Netherlands," *Int. J. Remote Sens.,* Vol. 14, 799–821, 1993.
19. Lavery, P., C. Pattiaratchi, A. Wyllie, and P. Hick, "Water quality monitoring in estuarine water using the Landsat Thematic Mapper," *Remote Sens. Environ.,* Vol. 46, 268–280, 1993.
20. Pulliainen, J., K. Kallio, K. Eloheimo, S. Koponen, et al., "A semi-operational approach to water quality retrieval from remote sensing data," *The Science of the Total Environment,* Vol. 268, 79–93, 2001.
21. Koponen, S., J. Pulliainen, H. Servomaa, Y. Zhang, et al., "Analysis on the feasibility of multi-source remote sensing observations for chl-a monitoring in Finnish lakes," *The Science of the Total Environment,* Vol. 268, 95–106, 2001.
22. Ulaby, F. T., *Microwave Remote Sensing: Active and Pas-*

sive, Vol. I, Addison-Wesley Publishing Company, Reading Massachusetts, 1981.

23. Nyfors, E. and P. Vainikainen, *Industrial Microwave Sensors,* Artech House, 1989.
24. Chen, K. S., A. K. Fung, and D. E. Weissmann, "A backscattering model for ocean surface," *IEEE Trans. Geosci. Remote Sens.,* Vol. 30, 811–817, 1992.
25. Broschat, S. L., "The small slope approximation reflection coefficient for scattering from a 'Pierson-Moskowitz' sea surface," *IEEE Trans. Geosci. Remote Sens.,* Vol. 31, 1112–1114, 1993.
26. Zhang, Y., S. Koponen, J. Pulliainen, and M. Hallikainen, "Turbidity and Secchi disk depth analysis derived from Landsat Thematic Mapper data combined with ERS-2 data in the Gulf of Finland," *The 2nd Int. Symposium Operationalization of Remote Sensing,* ITC, Enschede, The Netherlands, August 16–20, 1999.
27. Ouaidrari, H. and E. F. Vermote, "Operational atmospheric correction of Landsat TM data," *Remote Sens. Environ.,* Vol. 70, 4–15, 1999.
28. Zhang, M., K. Carder, F. E. Muller-Karger, Z. Lee, and D. B. Gold, "Noise reduction and atmospheric correction for coastal applications of Landsat Themtic Mapper," *Remote Sens. Environ.,* Vol. 70, 167–180, 1999.
29. Chavez Jr., P. S., "An improved dark-object subtraction technique for atmospheric scattering correction of multispectral data," *Remote Sens. Environ.,* Vol. 24, 459–479, 1988.
30. Chavez Jr., P. S., "Image-based atmospheric corrections-revised and improved," *Photogramm. Eng. Remote Sens.,* Vol. 62, 1025–1036, 1996.
31. Gilabert, M. A., C. Conese, and F. Maselli, "An atmospheric correction method for the automatic retrieval of surface reflectances from TM images," *Int. J. Remote Sens.,* Vol. 15, 2065–2086, 1994.
32. Ulaby, F. T., R. K. Moore, and A. K. Fung, "Radar remote sensing and surface scattering and emission theory," *Microwave Remote Sensing: Active and passive,* Vol. II, 853–860, Addison-Wesley Publishing Company, Reading Massachusetts, 1982.
33. Lindell, T., D. Pierson, G. Premazzi, and E. Zilioli, "Manual for monitoring European lakes using remote sensing techniques, (Luxembourg: Official Publications of the European Communities), EUR 18665 EN, 1999.
34. Eloheimo, K., T. Hannonen, P. Härmä, T. Pyhälahti, S. Koponen,

J. Pulliainen, and H. Servomaa, "Coastal monitoring using satellite, airborne and in situ data in the archipelago of Baltic Sea," *Proceed. 5th Int. Conference Remote Sens. Marine and Coastal Environ.,* San Diego, USA, Oct. 5–7, 1998.

35. Hallikainen, M., "Development of sensors and methods for remote sensing of Northern areas by HUT laboratory of space technology," *IEEE Geosci. Remote Sens. Newsletter, ISSN 0161-7869,* Vol. 107, 10–11, Dec. 1999.
36. Zhang, Y., S. Koponen, J. Pulliainen, and M. Hallikainen, "Landsat Thematic Mapper (TM) data analysis for chlorophyll-a and turbidity in the Gulf of Finland," *URSI/Remote Sensing Club of Finland/IEEE XXIII Convention on Radio Science and Remote Sensing Symposium,* 69–70, Espoo, Finland, August 24–25, 1998.
37. Zhang, Y., J. Pulliainen, S. Koponen, and M. Hallikainen, "Water quality retrievals from combined Landsat TM data and ERS-2 SAR data in the Gulf of Finland," *IEEE Trans. Geosci. Remote Sens.,* 2000 (submitted).
38. Bukata, R. P., J. H. Jerome, K. Y. A. Kondratyev, and D. V. Pozdnyakov, *Optical Properties and Remote Sensing of Inland Coastal Waters,* CRC Press Inc., Boca Raton, Florida, 1995.
39. Tassan, S., "Evaluation of the potential of the Thematic Mapper for marine application," *Int. J. Remote Sens.,* Vol. 8, 1455–1478, 1987.